

# Instability caused by the fermion-fermion interactions combined with rotational and particle-hole asymmetries in three-dimensional materials with quadratic band touching

Jing Wang<sup>1,2,\*</sup>

<sup>1</sup>*Department of Physics, Tianjin University, Tianjin 300072, P.R. China*

<sup>2</sup>*Department of Modern Physics, University of Science and Technology of China, Hefei, Anhui 230026, P.R. China*  
(Dated: November 7, 2021)

We investigate the role of four-fermion interactions, rotational and particle-hole asymmetries, and their interplay in three-dimensional systems with a quadratic band touching point by virtue of the renormalization group approach, which allows to treat all these facets unbiasedly. The coupled flow evolutions of interaction parameters are derived by taking into account one-loop corrections in order to explore the behaviors of low-energy states. We find four-fermion interaction can drive Gaussian fixed points to be unstable in the low-energy regime. In addition, the rotational and particle-hole asymmetries, together with the fermion-fermion interactions conspire to split the trajectories of distinct types of fermionic couplings and induce superconductivity instability with appropriate starting conditions. Furthermore, we present the schematic phase diagrams in the parameter space, showing the overall behaviors of states in the low-energy regime caused by both fermionic interactions and asymmetries.

PACS numbers: 73.43.Nq, 71.10.-w

## I. INTRODUCTION

Systems with a quadratic band touching (QBT) point in their electronic structures recently have become a much studied subject in condensed matter physics<sup>1–17</sup>. In a sharp contrast to the conventional Fermi metals owning a finite Fermi surface<sup>18</sup> or Dirac/Weyl semimetals possessing several discrete Dirac points and linear energy dispersions<sup>19</sup>, the two-dimensional (2D) QBT systems have a QBT point at which the density of states is finite<sup>3,5</sup> such as the bilayer graphene<sup>4,20–24</sup>. This unconventional structure of Fermi surface can bring a range of interesting phenomena, for instance the quantum anomalous Hall (QAH) effect<sup>25–27</sup> and quantum spin Hall (QSH) effect<sup>28–30</sup>. Recently, it has been found that both QAH and QSH can be stabilized in the checkerboard lattice model with a 2D QBT system by the short-ranged four-fermion interactions<sup>3,5</sup>. Several interesting behaviors and instabilities of these topological insulators in the presence of distinct sorts of impurities have also been examined and addressed in Ref.<sup>31</sup>. Besides the 2D QBT systems<sup>1–5,7,32</sup>, three-dimensional (3D) QBT electronic systems<sup>6,10–16,33–45</sup>, such as Luttinger semimetals<sup>33,34,42–45</sup>, have also attracted much attention due to their unconventional 3D dispersions of low-energy excitations and fermion-fermion interactions<sup>7–16,33,42–45</sup>.

In 3D QBT systems, such as gray tin, HgTe<sup>35</sup> or Luttinger semimetals<sup>33,34</sup>, the electron-electron interactions may result in non-Fermi liquid behaviors<sup>5,8–11,46</sup>. Additionally, the phase transitions/potential quantum phase transitions might be accompanied by lots of singular and interesting quantum critical behaviors in the vicinity of corresponding quantum critical point (QCP) at the low-energy regime<sup>8,10,11</sup>, which are closely related to the unconventional structure of Fermi surface and low-energy

energy dispersions in 3D QBT systems. In order to investigate the quantum criticality and unusually physical behaviors in 3D QBT systems, it is worth exploring whether the system harbors any fixed points and judging which fixed points are stable or unstable in the presence of different types of electron-electron interactions and rotational/particle-hole asymmetries in the low-energy regime. Fortunately, one usually can employ the powerful renormalization group (RG) approach<sup>47–50</sup> to seek the potential fixed points at the lowest-energy limit by treating distinct sorts of interactions on the same footing. After determining the potential (rescaled) fixed points<sup>4,5</sup> and stable fixed points in the low-energy regime, we can explore the associated physical behaviors in the low-energy regime and investigate the corresponding phase transitions/quantum phase transitions in the vicinity of these fixed points.

In this work, we study how the four-fermion interactions, rotational and particle-hole asymmetries, and their interplay influence the low-energy states of 3D QBT semimetal, which is a typically 3D electronic system with quadratic band touching<sup>7,8,10,11,39–41</sup>. To this end, we adopt the RG framework<sup>47–50</sup> to unbiasedly treat all possible effects and contributions. To be specific, the rotational and particle-hole asymmetries as well as all six short-ranged fermion-fermion interactions are considered at the same footing to derive the coupled flow equations of the interaction parameters. Based on these, we subsequently study the behaviors of low-energy states. Concretely, we, at the outset, only switch on the four-fermion interactions with preservation of rotational and particle-hole symmetries. After completing attentive RG analysis and numerically dealing with the associated coupled flow equations, we find that the short-ranged fermionic interaction can drive noninteracting Gaussian fixed point to become unstable and eventually flow to the strong cou-

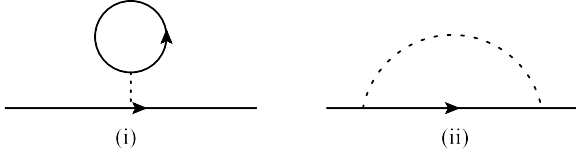


FIG. 1. One-loop corrections to the fermion propagator (the dashed line indicates the interactions).

pling in the low-energy regime as long as the initial values of these coupling are adequately large. Thereafter, the rotational and particle-hole asymmetries are also turned on. On one hand, the trajectories of distinct types of four-fermion couplings that are degenerated in the noninteracting situation are unambiguously split by the interplay between four-fermion interactions and asymmetries. On the other, we find there exists a relatively fixed point or critical point at certain critical energy scale as long as the starting conditions are satisfied. Superconductivity instability is always triggered and conventionally via approaching this fixed point. In order to obviously exhibit the overall behaviors of states in the low-energy regime, the schematic phase diagrams are provided upon varying the particle-hole and rotational asymmetric parameters  $\alpha$  and  $\delta$ .

The rest paper is organized as follows. In Sec. II, we provide our microscopic model and address the effective theory for 3D QBT semimetals. The Sec. III is accompanied to complete the one-loop RG analysis and derive the coupled flow equations of all fermion-fermion couplings. In Sec. IV, we numerically evaluate the correlated coupled equations and discuss the influence of four-fermion interaction on the low-energy states of 3D QBT systems. We next try to inspect the effects of low-energy states by incorporating into the contributions from both the six types of short-ranged fermionic interactions and rotational and particle-hole asymmetries in Sec. V. We finally present a short summary in Sec. VI.

## II. MODEL AND EFFECTIVE THEORY

Within this work, our focus is on the the following standard 3D QBT semimetals<sup>11,33</sup>, whose low-energy quasiparticle excitations and their interactions can be described by

$$\mathcal{L} = \psi^\dagger(\tau, \mathbf{x})(\partial_\tau + H_0)\psi(\tau, \mathbf{x}) + \sum_{i=0}^5 g_i [\psi^\dagger(\tau, \mathbf{x})\gamma_i\psi(\tau, \mathbf{x})]^2 \mathbf{1}$$

with  $\tau$  and  $\psi(\tau, \mathbf{x})$  respectively representing the imaginary time and four-component Grassmann field  $\psi(\tau, \mathbf{x}) = (\psi_1, \psi_2, \psi_3, \psi_4)^T$ . Here, the  $\gamma$  matrices, which stem from one of the (two possible) irreducible four-dimensional Hermitian representations<sup>10,11</sup>, own five components and satisfy the standard Clifford algebra  $\{\gamma_a, \gamma_b\} = 2\delta_{ab}$ ,  $a, b = 1-5$ . In addition,  $\gamma_0$  serves as the identity matrix.

We firstly consider the free terms of the low-energy quasiparticles, which can be expressed as

$$\mathcal{H}_0(\mathbf{p}) = \alpha \mathbf{p}^2 + \sum_{a=1}^5 d_a(\mathbf{p})\gamma_a + \delta \sum_{a=1}^5 s_a d_a(\mathbf{p})\gamma_a, \quad (2)$$

The parameters  $\alpha$  and  $\delta$  are directly linked to the Luttinger parameters<sup>11</sup>. It is worth pointing out that the particle-hole and rotational symmetries/asymmetries of systems are closely associated with the values of parameters  $\alpha$  and  $\delta$ , respectively. To be specific, the physical systems harbor both particle-hole and rotational symmetries<sup>7,10,11</sup> once both of two parameters  $\alpha$  and  $\delta$  are tuned to 1 and 0, namely  $\alpha_s \equiv 1$  and  $\delta_s \equiv 0$ , respectively. On the contrary, as long as the symmetric values of  $\alpha$  and/or  $\delta$  are deviated, particle-hole and/or rotational asymmetries are developed simultaneously. Here, the  $d_a(\mathbf{p})$  factor possesses a general form in  $d$  dimension<sup>10,11</sup>

$$d_a(\mathbf{p}) = \sqrt{\frac{d}{2(d-1)}} p_i \Lambda_{ij}^a p_j, \quad (3)$$

with  $\Lambda_{ij}^a$  representing a  $d \times d$  Gell-Mann matrices<sup>10,11</sup>. Utilizing the same conventions in Ref.<sup>11</sup>, we choose  $s_a = 1$  for the off-diagonal (indices 2,3,4) and  $s_a = -1$  for the diagonal (indices 1,5) matrices. Concretely, the five functions  $d_a(\mathbf{p})$  in Eq. (2) can be designated for our  $d = 3$  model by exploiting the real  $l = 2$  spherical harmonics as<sup>7,10,11</sup>

$$\begin{aligned} d_1(\mathbf{p}) &= \frac{\sqrt{3}}{2}(p_x^2 - p_y^2), \\ d_2(\mathbf{p}) &= \sqrt{3}p_x p_y, \\ d_3(\mathbf{p}) &= \sqrt{3}p_x p_z, \\ d_4(\mathbf{p}) &= \sqrt{3}p_y p_z, \\ d_5(\mathbf{p}) &= \frac{1}{2}(2p_z^2 - p_x^2 - p_y^2). \end{aligned} \quad (4)$$

In addition, the last term of Eq. (1) captures all potential four-fermion interactions of the low-energy quasiparticles, which will be focused in Sec. III. The one-loop RG analysis of our model (1) will be practiced in forthcoming two sections for both symmetric and asymmetric cases.

## III. RG ANALYSIS AND COUPLED FLOW EQUATIONS

Before performing a standard RG analysis, it is convenient to rescale the momenta and energy by  $\Lambda_0$  which is tied to the lattice constant, i.e.  $\mathbf{p} \rightarrow \mathbf{p}/\Lambda_0$  and  $\omega \rightarrow \omega = \omega/\Lambda_0^2$ , and designate the energy scale as  $\Lambda = \Lambda_0/b$  with  $b = e^{-l}$  and  $l \geq 0$ <sup>47-62</sup> to represent the evolution of energy scales. Next, we are going to extract the contributions from these one-loop diagrams and derive the coupled flow equations for the interaction parameters.

Before moving further, it is of very importance to emphasize that the RG evolutions of interaction parameters are closely associated with the free fixed point, which determines the basic RG rescalings of energies, momenta, and fields. In this work, we make  $S_0 \sim i\omega + \sum_{a=1}^5 d_a(\mathbf{p})\gamma_a$  invariant under RG transformation as the free fixed point and correspondingly the rescalings are

$$\omega \rightarrow \omega' e^{-2l}, \quad (5)$$

$$p_i \rightarrow p'_i e^{-l}, \quad (6)$$

$$\psi(\omega, \mathbf{p}) \rightarrow \psi'(\omega', \mathbf{p}') e^{7/2l}. \quad (7)$$

According to these points, the parameters  $\alpha$  and  $\delta$  are two constants at the tree level. Further, as the one-loop corrections from four-fermion interactions do not contribute to the self-energy, one can easily figure out that they both are still energy-independent at least to one-loop level. As a consequence, we within this work regard these two parameters as two constants that are assumed to be linked to distinct physical situations among many others.

### A. In the presence of the rotational and particle-hole symmetries

We firstly go to investigate the system in the presence of both the rotational and particle-hole symmetries. In such circumstances, the free term  $H_0$  in Eq. (2) is reduced to the compact form

$$\mathcal{H}_0(\mathbf{p}) = \sum_{a=1}^5 d_a(\mathbf{p})\gamma_a, \quad (8)$$

where  $d_a(\mathbf{p}) \equiv \mathbf{p}^2 \tilde{d}_a(\Omega)$  with  $a = 1 - 5$  has already been introduced in Eq. (4). This defines the real hyperspherical harmonics  $\tilde{d}_a(\Omega)$  for angular momentum of two in general dimension, with  $\Omega$  denoting the spherical angles on the  $(d-1)$  sphere in  $\mathbf{p}$  space<sup>7,10,11</sup>. After performing corresponding Fourier transformations by adopting our starting point (1), we obtain the revised effective action

$$S = \int_{-\infty}^{+\infty} \frac{d\omega}{2\pi} \int^\Lambda \frac{d^d \mathbf{p}}{(2\pi)^d} \psi^\dagger(\omega, \mathbf{p}) \left[ i\omega + \sum_{a=1}^5 d_a(\mathbf{p})\gamma_a \right] \psi(\omega, \mathbf{p}) + \sum_{i=0}^5 g_i \int_{-\infty}^{+\infty} \frac{d\omega_1 d\omega_2 d\omega_3}{(2\pi)^3} \int^\Lambda \frac{d^d \mathbf{p}_1 d^d \mathbf{p}_2 d^d \mathbf{p}_3}{(2\pi)^{3d}} \\ \times \psi^\dagger(\omega_1, \mathbf{p}_1) \gamma_i \psi(\omega_2, \mathbf{p}_2) \psi^\dagger(\omega_3, \mathbf{p}_3) \gamma_i \psi(\omega_1 + \omega_2 - \omega_3, \mathbf{p}_1 + \mathbf{p}_2 - \mathbf{p}_3), \quad (9)$$

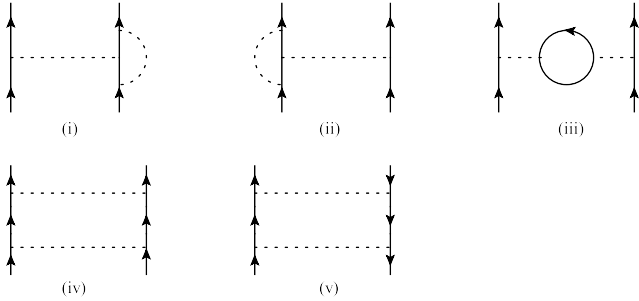


FIG. 2. One-loop corrections to the fermion interacting couplings (the dashed line indicates the interactions).

which straightforwardly gives rise to the free fermion propagator<sup>10,11</sup>,

$$G_0(\omega, \mathbf{p}) = \frac{-i\omega + \sum_{a=1}^5 d_a(\mathbf{p})\gamma_a}{\omega^2 + \mathbf{p}^4}. \quad (10)$$

Subsequently, we derive the coupled flow equations of the parameters after considering the one-loop corrections in Fig. 1 and Fig. 2 and carrying out the standard RG analysis<sup>49-57</sup>,

$$\frac{dg_0}{dl} = -g_0 - \frac{g_0 \mathcal{F}_0}{5\pi^2}, \quad (11)$$

$$\frac{dg_a}{dl} = -g_a + \frac{4g_a(g_0 - \mathcal{F}_0) - \mathcal{F}_1}{10\pi^2}. \quad (12)$$

### B. In the absence of the rotational and particle-hole symmetries

We then move to the asymmetric situations. In the absence of the rotational and particle-hole symmetries, we have the general effective free Hamiltonian as given in Eq. (2) with the restricted conditions  $\delta \neq \delta_s$  and  $\alpha \neq \alpha_s$ <sup>7,10,11</sup>. The free fermion propagator can be corre-

spondingly extracted as<sup>10,11</sup>,

$$G_0(\omega, \mathbf{p}) = \frac{1}{i\omega + \alpha \mathbf{p}^2 + \sum_{a=1}^5 (1 + \delta s_a) d_a(\mathbf{p}) \gamma_a}, \quad (13)$$

with the asymmetric parameters  $\alpha \neq \alpha_s$  and  $\delta \neq \delta_s$ . In order to simplify further expressions and calculations, we here derive and designate some useful identities by employing Eq. (4),

$$\sum_{a=1}^5 [d_a(\mathbf{p}) \gamma_a]^2 = (p_z^2 + p_x^2 + p_y^2)^2 = \mathbf{p}^4, \quad (14)$$

and

$$\begin{aligned} & \sum_{a=1}^5 (1 + \delta s_a)^2 [d_a(\mathbf{p}) \gamma_a]^2 \\ &= (1 - \delta)^2 (p_x^4 + p_y^4 + p_z^4) + 2(1 + 4\delta + \delta^2) \\ & \quad \times (p_x^2 p_y^2 + p_x^2 p_z^2 + p_y^2 p_z^2) \\ &\equiv \mathbf{p}_\delta^4. \end{aligned} \quad (15)$$

To proceed, we can derive the coupled flow equations for general values of  $\alpha$  and  $\delta$ , which result in the rotational and particle-hole asymmetries via paralleling and performing the similar procedures of the rotational and particle-hole symmetry case as shown in Sec. III A,

$$\frac{dg_0}{dl} = -g_0 - \frac{1}{16\pi^3} \left[ g_0(\mathcal{F}_0 - g_0) \mathcal{N}_{+++++} + g_0(g_1 + g_5) \mathcal{M}_3 + g_0(g_2 + g_3 + g_4) \mathcal{M}_2 + \frac{1}{2} \mathcal{F}_1 \mathcal{M}_1 \right], \quad (16)$$

$$\begin{aligned} \frac{dg_1}{dl} = -g_1 - \frac{1}{16\pi^3} & \left[ -2g_1^2 \mathcal{N}_{+-----} + g_1(g_0 + 2g_1 - \mathcal{F}_0) \mathcal{N}_{++++-} + g_1[g_0 \mathcal{M}_1 + g_5 \mathcal{M}_5 \right. \\ & \left. + (g_2 + g_3 + g_4) \mathcal{M}_4] + \frac{1}{2} \mathcal{F}_1 \mathcal{M}_3 \right], \end{aligned} \quad (17)$$

$$\frac{dg_2}{dl} = -g_2 - \frac{1}{16\pi^3} \left[ g_2(g_0 - \mathcal{F}_0) \mathcal{N}_{-+----} + g_2[g_0 \mathcal{M}_1 + (g_1 + g_5) \mathcal{M}_5 + (g_3 + g_4) \mathcal{M}_4] + \frac{1}{2} \mathcal{F}_1 \mathcal{M}_2 \right], \quad (18)$$

$$\frac{dg_3}{dl} = -g_3 - \frac{1}{16\pi^3} \left[ g_3(g_0 - \mathcal{F}_0) \mathcal{N}_{--+-} + g_3[g_0 \mathcal{M}_1 + (g_1 + g_5) \mathcal{M}_5 + (g_2 + g_4) \mathcal{M}_4] + \frac{1}{2} \mathcal{F}_1 \mathcal{M}_2 \right], \quad (19)$$

$$\frac{dg_4}{dl} = -g_4 - \frac{1}{16\pi^3} \left[ g_4(g_0 - \mathcal{F}_0) \mathcal{N}_{----+} + g_4[g_0 \mathcal{M}_1 + (g_1 + g_5) \mathcal{M}_5 + (g_2 + g_3) \mathcal{M}_4] + \frac{1}{2} \mathcal{F}_1 \mathcal{M}_2 \right], \quad (20)$$

$$\frac{dg_5}{dl} = -g_5 - \frac{1}{16\pi^3} \left[ g_5(g_0 - \mathcal{F}_0) \mathcal{N}_{-----} + g_5[g_0 \mathcal{M}_1 + g_1 \mathcal{M}_5 + (g_2 + g_3 + g_4) \mathcal{M}_4] + \frac{1}{2} \mathcal{F}_1 \mathcal{M}_3 \right]. \quad (21)$$

Again, the first and second terms of above RG equations that collect tree-level and one-loop level corrections of fermion-fermion interactions are linear and quadratic, respectively. Please refer to the paragraph below Eq. (12) for detailed information. In order to write the coupled equations as the compact forms, we here bring out several new coefficients in above coupled running Eqs. (16)-(21). The defined parameters/functions  $\mathcal{F}_0$  and  $\mathcal{F}_1$  have already been provided in Eqs. 11 and 12 and  $\mathcal{M}_i$  with

$i = 1 - 5$  are nominated as follows,

$$\mathcal{M}_{\mathbb{F}} = \int_{x, \theta, \varphi} \frac{64 \sin^2 \theta [\alpha^2 (\alpha^2 - f_\delta + x^2)]}{[(\alpha^2 - f_\delta - x^2)^2 + 4x^2 \alpha^2]^2}, \quad (22)$$

$$\mathcal{M}_{\mathbb{F}} = \int_{x, \theta, \varphi} \frac{64 \sin^2 \theta [(\alpha^2 - f_\delta - x^2)^2] (1 + \delta)^2 f_{d_C}^2}{[(\alpha^2 - f_\delta - x^2)^2 + 4x^2 \alpha^2]^2}, \quad (23)$$

$$\mathcal{M}_{\mathbb{F}} = \int_{x, \theta, \varphi} \frac{64 \sin^2 \theta [(\alpha^2 - f_\delta - x^2)^2] (1 - \delta)^2 f_{d_C}^2}{[(\alpha^2 - f_\delta - x^2)^2 + 4x^2 \alpha^2]^2}, \quad (24)$$

$$\mathcal{M}_{\mathbb{F}} = \int_{x, \theta, \varphi} \frac{\sin^2 \theta \left\{ 32 [-8\alpha^2 x^2] (1 + \delta)^2 f_{d_C}^2 \right\}}{[(\alpha^2 - f_\delta - x^2)^2 + 4x^2 \alpha^2]^2}, \quad (25)$$

$$\mathcal{M}_{\mathbb{F}} = \int_{x, \theta, \varphi} \frac{\sin^2 \theta \left\{ 32 [-8\alpha^2 x^2] (1 - \delta)^2 f_{d_C}^2 \right\}}{[(\alpha^2 - f_\delta - x^2)^2 + 4x^2 \alpha^2]^2}, \quad (26)$$

with introducing

$$\int_{x,\theta,\varphi} \equiv \int_{-\infty}^{+\infty} \frac{dx}{(2\pi)} \int_0^\pi d\theta \int_0^{2\pi} d\varphi. \quad (27)$$

Here the coefficients for  $f_\delta$  and  $f_{d_a^2}$  with  $a = 1 - 5$  are given by

$$f_\delta = [2(1 + 4\delta + \delta^2)(\sin^4 \theta \cos^2 \varphi \sin^2 \varphi + \sin^2 \theta \cos^2 \theta) + (1 - \delta)^2(\sin^4 \theta \cos^4 \varphi + \sin^4 \theta \sin^4 \varphi + \cos^4 \theta)], \quad (28)$$

$$f_{d_1^2} = 3(\sin^2 \theta \cos^2 \varphi - \sin^2 \theta \sin^2 \varphi)^2 / 4, \quad (29)$$

$$f_{d_2^2} = 3 \sin^4 \theta \sin^2 \varphi \cos^2 \varphi, \quad (30)$$

$$f_{d_3^2} = 3 \sin^2 \theta \cos^2 \theta \cos^2 \varphi, \quad (31)$$

$$f_{d_4^2} = 3 \sin^2 \theta \cos^2 \theta \sin^2 \varphi, \quad (32)$$

$$f_{d_5^2} = (2 \cos^2 \theta - \sin^2 \theta)^2 / 4. \quad (33)$$

In addition, the coefficients  $\mathcal{N}(\xi_1 \xi_2 \xi_3 \xi_4 \xi_5)$  are designated as

$$\begin{aligned} & \mathcal{N}(\xi_1 \xi_2 \xi_3 \xi_4 \xi_5) \int_{x,\theta,\varphi} \frac{\sin^2 \theta}{[(\alpha^2 - f_\delta - x^2)^2 + 4x^2 \alpha^2]^2} \\ & \times \left\{ 4[-x^2(\alpha^2 + f_\delta + x^2)^2 + \alpha^2(\alpha^2 - f_\delta - x^2)^2 + 4\alpha^2 x^2 \right. \\ & \times (\alpha^2 - f_\delta)] + 4[(\alpha^2 - f_\delta - x^2)^2 - 4\alpha^2 x^2][3(1 + \delta)^2 \\ & \times (\xi_2 f_{d_2^2} + \xi_3 f_{d_3^2} + \xi_4 f_{d_4^2}) + 2(1 - \delta)^2(\xi_1 f_{d_1^2} + \xi_5 f_{d_5^2})] \Big\}. \quad (34) \end{aligned}$$

Hereby, we highlight that the five signs  $\xi_i = \pm$  corresponds to the signs of terms  $f_{d_i^2}$  with  $i = 1 - 5$ , respectively.

#### IV. ROLE OF FOUR-FERMION INTERACTION IN THE LOW-ENERGY STATES FOR THE SYMMETRIC SITUATIONS

In the previous section III, we have derived the coupled flow equations for interaction parameters via clinching the interplay among different four-fermion parameters and information of rotational and particle-hole symmetries. In the spirit of RG, the low-energy behaviors of systems can be conventionally extracted from these equations. Accordingly, we now are in a suitable position to reveal the influence of interplay among distinct four-fermion couplings on the low-energy properties of the 3D QBT systems.

It is well known that the order parameters or quasi-particles in the most of condensed matter systems are inescapably coupled and mutually influenced due to the strong quantum fluctuations nearby the QCP in the low-energy regime<sup>50,63-65</sup>. This immediately raises a question that whether and how the QCP is slightly revised or completely changed by the interplay between distinct quartic couplings in the low-energy regime?

Before going further, we would like stress that there exists two distinct situations, which are distinguished by presence or absence of the rotational and particle-hole

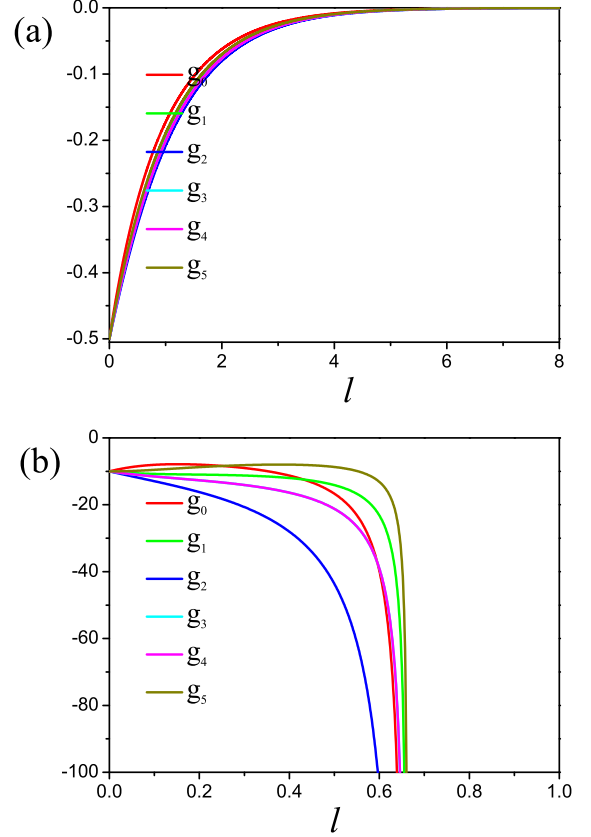


FIG. 3. (Color online) Four-fermion couplings flow to: (a) the Gaussian fixed point for small initial values with  $g_i(l=0) < 0$  (the basic results are the same for  $g_i(l=0) > 0$  and not shown here); and (b) strong coupling for large initial values with  $g_i(l=0) < 0$ . All the energy-dependent evolutions are measured by the  $\Lambda_0^{-1}$ .

symmetries. For the asymmetric cases, the rotational and/or particle-hole symmetries would be broken and the asymmetries are representatively measured by the parameters  $\alpha$  and  $\delta$ , with which the associated flow equations of four-fermion couplings are presented in Eq. (16)-(21). In a sharp contrast, the system preserves both the rotational and particle-hole symmetries for the symmetric situations, which we put our focus on within this section. To proceed, the corresponding evolutions are given by Eqs. (11)-(12). These fermion-fermion parameters in Eq. (1),  $g_i$  with  $i = 0$  to 5, manifestly become energy-dependent and are restricted by each other upon lowering the energy scale. After incorporating into the intimate influence of these fermionic couplings, the correlatedly four-fermion parameters in Eq. (1),  $g_i$ ,  $i = 0 - 5$ , become closely energy-dependent and are restricted by coupled flow equations upon lowering the energy scale. With the respect to the rotational and particle-hole symmetries, we are informed that the parameters  $\alpha = \alpha_s$  and  $\delta = \delta_s$ . Concretely, we utilize the corresponding RG equations (11)-(12) and arrive at the results as depicted in Fig. 3



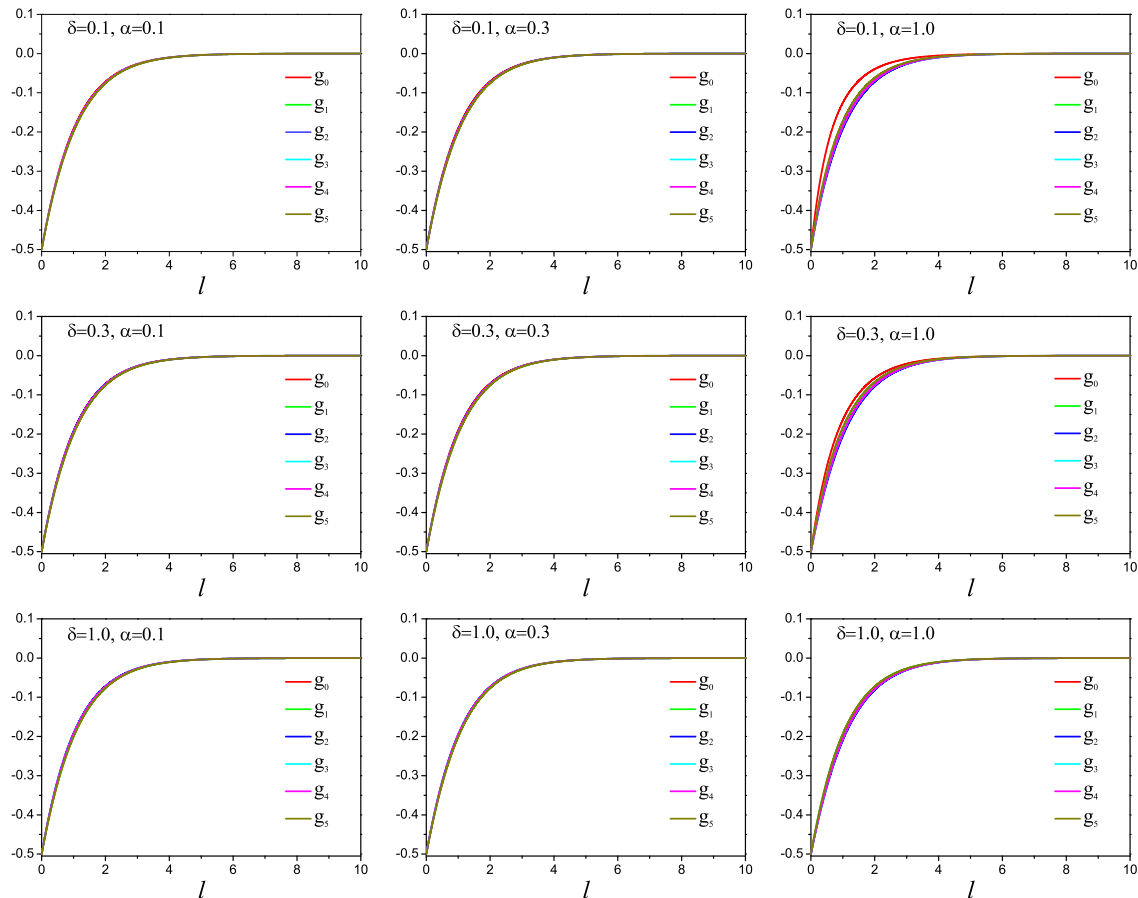


FIG. 4. (Color online) Evolutions of four-fermion couplings for the small initial values with  $g_i(l=0) < 0$  with  $i = 0 - 5$  (the basic results are the same for  $g_i(l=0) < 0$ ) and several representative values of asymmetric parameters  $\delta$  and  $\alpha$ . All the energy-dependent evolutions are measured by the  $\Lambda_0^{-1}$  (the flows of couplings  $g_2$  and  $g_3$  are nearly overlapped).

after performing the straightforwardly numerical calculations. Studying from Fig. 3(a), we obtain that all four-fermion couplings flow towards zero at the lowest energy limit if the initial values of  $|g_i(l=0)|$ ,  $i = 0 - 5$ , are sufficiently small. This clearly indicates that the system under some starting situations runs to the Gaussian fixed point at the lowest energy limit although the mutual influence among distinct coupling are switched on. However, the Gaussian fixed point is no longer stable and qualitatively moved by the four-fermion interactions if the initial values of  $|g_i(l=0)|$ ,  $i = 0 - 5$ , are adequately large as demonstrated in Fig. 3(b). To be specific, all the couplings parameters flows away from the Gaussian fixed point. In particular, it is interesting to point out the evolutions of  $g_i$  with  $i = 1 - 5$  are overlapped due to their RG equations taking the similar structure as shown in Eq. 12. Gathering the information of this subfigure, we unambiguously find that the Gaussian fixed point is changed qualitatively and all the four-fermion parameters  $g_i$ ,  $i = 0 - 5$ , flow towards the strong couplings at the lowest-energy limit.

To be brief, it is worth pointing out that there are sev-

eral interesting points are triggered by the four-fermion interactions. In variance with the noninteracting circumstance, the Gaussian fixed point can either be reached if the initial values of fermionic parameters are small or qualitatively destroyed and flow towards strong coupling when their starting values are sufficiently large. Therefore, the QCP in noninteracting case is erased and replaced by the strong couplings if the four-fermion interactions are turned on.

## V. EFFECTS OF INTERACTIONS COMBINED WITH ASYMMETRIES ON THE LOW-ENERGY STATES

As presented in previous section, the low-energy states of 3D QBT somehow, even for the preservation of rotational and particle-hole symmetries, can be revised by the mutual interactions among different types of four-fermion couplings. One maybe naturally ask further what about the roles of rotational and particle-hole asymmetries in the low-energy behaviors meanwhile these four-fermion

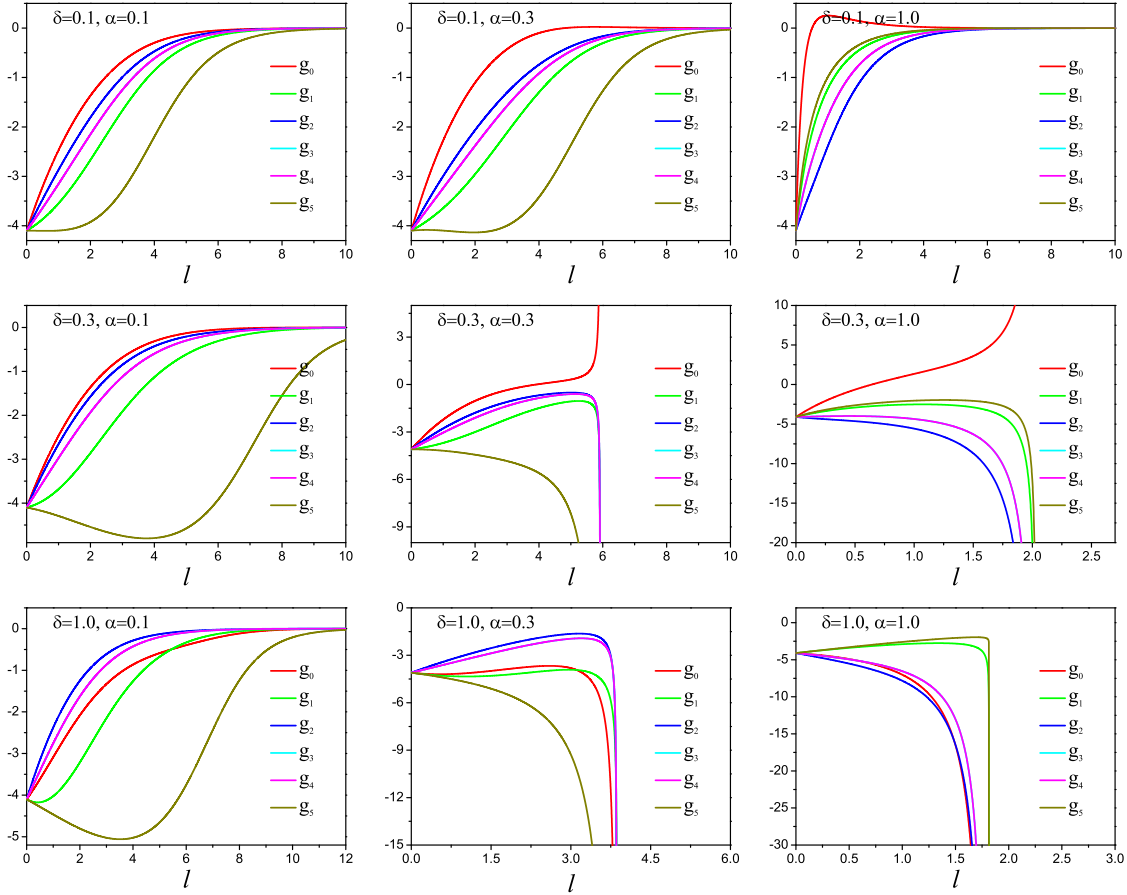


FIG. 5. (Color online) Evolutions of four-fermion couplings for the moderate initial values with  $g_i(l=0) < 0$  and distinct values of asymmetric parameters  $\delta$  and  $\alpha$ . All the energy-dependent evolutions are measured by the  $\Lambda_0^{-1}$  (the flows of couplings  $g_2$  and  $g_3$  are nearly overlapped).

interactions are switched on. We are going to investigate these in the rest of this section.

### A. Split evolutions of interaction parameters

In order to study the general case in which the rotational and particle-hole symmetries cannot always be preserved, we are forced to transfer our focus from the coupled flow equations Eqs. (11)-(12) to the asymmetric situations, namely Eqs. (16)-(21), which are derived from the presence of general values of  $\alpha$  and  $\delta$ . By carrying out the analogous procedures, we respectively summarized the primary results in Fig. 4 and Fig. 5 for small and large initial values of four-fermion couplings and several selected values of asymmetric parameters.

We here would like to discuss the behaviors of trajectories for fermionic couplings influenced by  $\alpha$  and  $\delta$ , leaving the study of fixed points in the following subsection. Collecting the information of Fig. 4 and Fig. 5, we find that, although the final destination may be not changed, the energy-dependent trajectories of fermionic couplings are

stretched to be split no matter their starting values are small or large. These behaviors are sharply compared to the overlapped trajectories in noninteracting case, in particular for small starting values of four-fermion couplings as compared to Fig. 3(a). This is apparently delineated in Fig. 4 and the separations among these five distinct interaction parameters are evidently broadened upon increasing the values of  $\alpha$  and  $\delta$ . Moreover, the split distance is increasingly separated as the asymmetric parameters  $\alpha$  and  $\delta$  are tuned to be large. Based on these, we therefore ascribe this split of fermion-fermion couplings to the role of rotational and particle-hole asymmetries.

### B. Instability

As already presented in Sec. IV, the rotational and particle-hole asymmetries can play an important role in the low-energy behaviors. However, it is necessary to collect the contribution from both the four-fermion interactions and asymmetries, which together determine the fate of 3D QBT system at the lowest-energy limit.

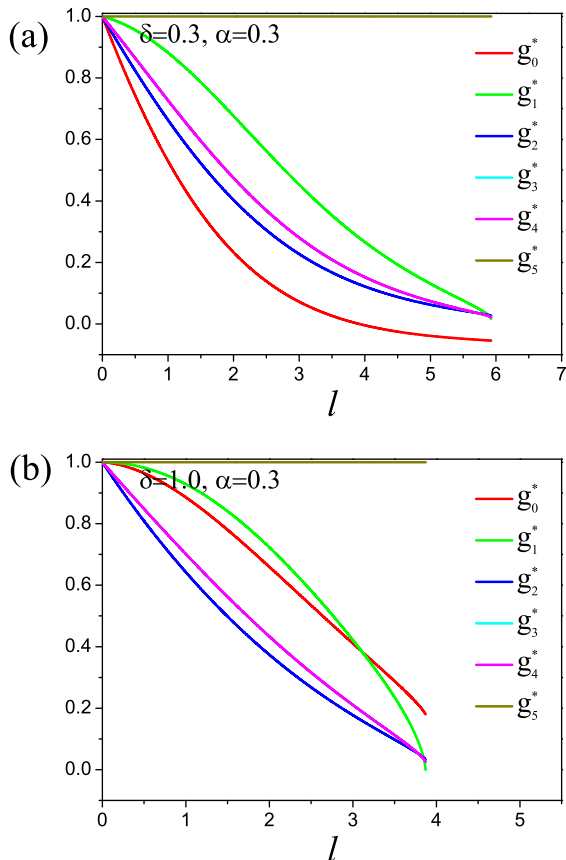


FIG. 6. (Color online) Relatively fixed point at the lowest-energy limit at some representative values of asymmetric parameters: (a)  $\delta = 0.3$  and  $\alpha = 0.3$  and (b)  $\delta = 1.0$  and  $\alpha = 1$ . The rescaled parameters  $g_i^*(l) = g_i(l)/g_5(l)$ ,  $i = 0, 1, 2, 3, 4, 5$  (the flows of couplings  $g_3$  and  $g_4$  are nearly degenerated).

At the start, we assume the initial values of fermionic couplings are very small and subsequently arrive at the results depicted in Fig. 4 by tuning the parameters of asymmetries. Studying from Fig. 4, it is worth pointing out that this principal results are insensitive to the values of  $\alpha$  and  $\delta$  that measure the rotational and particle-hole asymmetries. We subsequently move to the case with large initial values of four-fermion couplings. Paralleling the analogous procedures in Sec. IV gives rise to the same conclusion as exhibited in Fig. 3(b), namely the unstable of Gaussian fixed point. Finally, we would like to investigate the situation with “moderate initial values”, which can not trigger instability of Gaussian fixed point of fermion-fermion parameters at the symmetric case with  $\alpha = \alpha_s$  and  $\delta = \delta_s$ , namely belonging to class of Fig. 3(a). After carrying out the similar steps, we are informed that the energy-dependent coupling parameters  $g_i$ ,  $i = 0 - 5$  are intimately susceptible to the asymmetric values of  $\alpha$  and  $\delta$  as manifestly presented in Fig. 5 after paralleling the steps of previous case and numerically evaluating coupled running Eqs. (16)-(21) with large ini-

tial values of interaction parameters  $|g_i(l = 0)|$ . To be specific, the four-fermion parameters  $g_i$ ,  $i = 0 - 5$ , in analogous to Fig. 4, still flow to the Gaussian fixed point if the asymmetric values of  $\alpha$  and  $\delta$  are small enough as clearly exhibited in the first column of Fig. 5. As long as the asymmetric values of  $\alpha$  and  $\delta$  are increased, the behaviors of quartic couplings can be completely changed. As presented in the third column of Fig. 5, the Gaussian fixed point is entirely destroyed by the asymmetries and the coupling parameters  $g_i$ ,  $i = 0 - 5$  go towards the strong coupling at the lowest-energy limit. In distinction to the previous studies<sup>8</sup> where  $g_0$  is stable, our results suggest that there is no any QCP but instability towards the strong coupling caused by the contributions from the mutual competition between the four-fermion interactions and rotational and particle-hole asymmetries in the low-energy.

In variance with the case in the absence of the interplay between distinct parameters, several interesting results are captured after taking into account the fermion-fermion interactions. Before going further, we would like to present some comments on these. To recapitulate, the system can either go to the Gaussian fixed point or instability towards the strong coupling. In the presence of the rotational and particle-hole symmetries, the Gaussian fixed point would be broken and interaction parameters flow to the strong coupling by sufficiently large values of the initial interaction strengths as exhibited in Fig. 3(b). Furthermore, the behaviors of four-fermion couplings are sensitive to the values of asymmetries  $\alpha$  and  $\delta$  as the system does not possess the rotational and particle-hole symmetries. While the values of parameters  $\alpha$  and  $\delta$  are small, the instability hardly happens and the system always flows to the Gaussian fixed point as depicted in the first column of Fig. 5. However, the Gaussian fixed point would be destroyed totally and the system goes towards certain instability if the values of  $\alpha$  and  $\delta$  are adequately large as shown in the third column of Fig. 5.

### C. Fixed points and dominant phases

In order to elucidate more properties of these instabilities, we are suggested to seek the relatively fixed points at the strong coupling regime. Commonly, the phase transitions/potential quantum phase transitions are always closely linked to certain fixed points of interaction parameters in the low-energy regime, which are conventionally accompanied by a multitude of singular and critical behaviors in the low-energy regime<sup>8,10,11</sup>. In this respect, it is instructive to explore whether our system harbors any fixed points with the evolutions of four-fermion parameters. To this end, we rescale all four-fermion interaction parameters with one of them<sup>4,5,31</sup>, for instance  $g_5$ , to seek whether there exists any relatively fixed points in the parameter space described by the evolutions of  $g_i/g_5$ ,  $i = 0 - 5$  and further investigate the physical implications for



the tendency of strong couplings for the fermionic couplings. To proceed, we derive and plot the relative trajectories for  $g_i/g_5$  upon lowering the energy scale by means of paralleling the method and analysis in last two subsections. After carrying out several numerical calculations, we transfer the strong coupling tendencies in Fig. 3(b) and third column of Fig. 5 for both symmetric and asymmetric cases into the relative flows by rescaling all four-fermion parameters by  $g_5$  as displayed in Fig. 6. According to these results, we are informed that the system indeed owns two kinds of relatively fixed points (RFP), namely  $(g_0^*, g_1^*, g_2^*, g_3^*, g_4^*, g_5^*)_{\text{RFP-I}} \approx (-0.054, 0.017, 0.027, 0.022, 0.022, 1.00)$  for  $\delta = 0.3, \alpha = 0.3$  and  $(g_0^*, g_1^*, g_2^*, g_3^*, g_4^*, g_5^*)_{\text{RFP-II}} \approx (0.180, 0, 0.033, 0.025, 0.025, 1.00)$  for  $\delta = 0.1, \alpha = 1$ .

Generally, the interaction parameters evolving to the strong couplings or the existence of RFPs at certain critical energy scale  $l_c$  indicates the emergence of some instability with the divergent susceptibilities of order parameters<sup>4,5,66–72</sup>. To be specific, one can directly expect the emergence of superconductivity instability once the system goes towards the RFP-II attesting to the strong couplings of attractive fermion-fermion interactions<sup>11,49,69</sup>. In other words, the superconductivity instability is linked to the dominant phase. Next, we turn to the situation at which the RFP-I is achieved. Being different from the RFP-II, the parameter flows  $g_0$  is positively divergent upon approaching this RFP. However, we stress that the leading phase is still associated with the superconductivity instability. This conclusion is supported by two points. On one hand, although the parameter  $g_0$  diverges positively, its coupling  $(\psi^\dagger \gamma_0 \psi)^2$  conventionally corresponds to no order<sup>5</sup> and is considered as a role of chemical potential. Consequently, phase transition and dominant phase are insusceptible to the divergence of  $g_0$  no matter it is positive or negative. On the other hand, the parameter  $g_5$  that diverges negatively is the leading one at RFP-I in that its absolute value is the largest among all parameters. This means the attractive fermion-fermion interaction is preferred at the low-energy limit, pointing to the superconductivity instability<sup>11,49,69</sup>.

Based on all above analysis, we infer that the strong couplings of these four-fermion parameters can be generated via two distinct mechanisms in the presence of fermion-fermion interactions and asymmetries, which might be both mutually influenced and competed. On one hand, one can strengthen the initial values of fermionic coupling parameters to induce the strong coupling flows even at  $\alpha = \alpha_s$  and  $\delta = \delta_s$ . On the other, while the initial values of interaction parameters are inadequately large to destroy the Gaussian fixed point, the rotational and particle-hole asymmetries with  $\alpha \neq \alpha_s$  and/or  $\delta \neq \delta_s$  can potentially break the Gaussian fixed point and some instability takes place with the fermionic couplings running towards the strong coupling with the superconductivity instability at the lowest-energy limit. Additionally, we find that the critical coupling strength

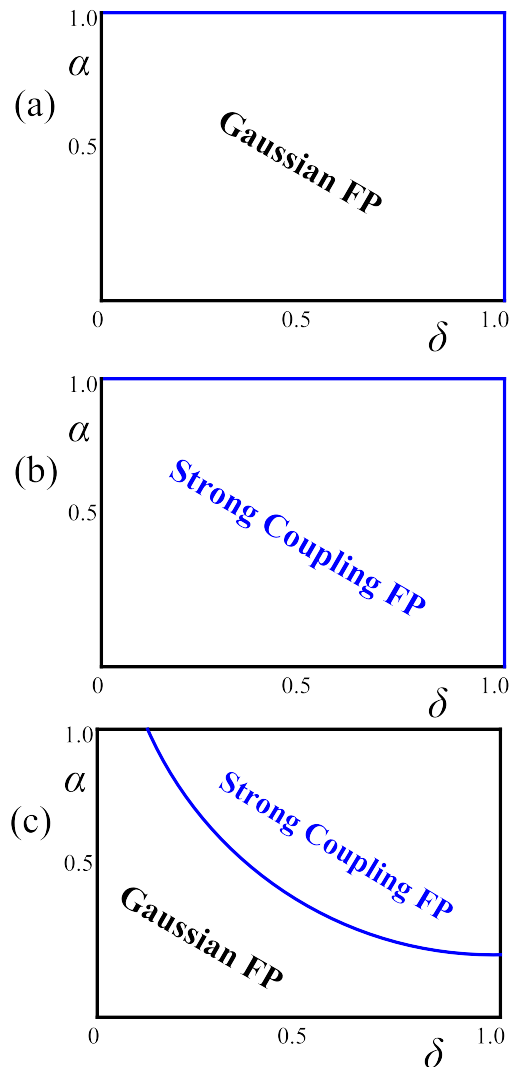


FIG. 7. (Color online) The schematic phase diagrams for potential fixed points at the lowest-energy limit in  $\alpha - \delta$  plane for (a) small initial values; (b) large initial values; and (c) moderate initial values of interaction parameters. The strong coupling is linked to the superconductivity instability and abbreviation “FP” designates the fixed point.

which induces the instability is much enhanced compared to the previous results<sup>8</sup>. In order to clearly exhibit the influence of asymmetries on the physical behaviors and fixed points and the difference between symmetric and asymmetric cases at the lowest-energy limit, we have plotted a phase diagram as presented in Fig. 7 to overall summarize these conclusions.

## VI. SUMMARY

In summary, we access the 3D QBT systems with certain quadratic band touching point<sup>7–13</sup>. How the low-energy behaviors of system would be revised by the distinct sorts of fermion-fermion interactions, rotational and

particle-hole asymmetries, and their interplay are attentively studied on the same footing by adopting the RG approach<sup>49,50</sup>. Not only all six potential short-ranged fermion-fermion couplings are equally involved, but also both symmetric and asymmetric cases are taken into account.

The coupled flow equations of all interaction parameters for both presence and absence of rotational and particle-hole symmetries are explicitly addressed after performing the detailed RG analysis by collecting the interplay between different fermionic couplings and asymmetries. Beginning with these running equations, we can study the behaviors of low-energy states. Initially, we find, switching on the four-fermion interactions with rotational and particle-hole symmetries, that the QCP in noninteracting case is destroyed and replaced by the strong couplings if the initial values of fermionic parameters are relative large. Subsequently, we turn on the rotational and particle-hole asymmetries. The split of the trajectories of distinct types of four-fermion couplings are

unambiguously stretched separately by the interplay between interaction and asymmetries. In addition, certain fixed point/critical point can be induced under certain conditions, at which the superconductivity instability is conventionally generated. To apparently display the role of asymmetries in the physical behaviors and fixed points as well as the difference between symmetric and asymmetric cases at the lowest-energy limit, we have provided a schematic phase diagram provided in Fig. 7.

## ACKNOWLEDGEMENTS

J.W. is supported by the National Natural Science Foundation of China under Grant No. 11504360 and acknowledges Dr. Dmitry V. Efremov, Dr. Carmine Ortix, and Prof. Jeroen van den Brink, for correlated collaborations and helpful discussions as well as Prof. W. Liu for useful discussions.

- 
- \* E-mail address: jing.wang@tju.edu.cn
- <sup>1</sup> Y. D. Chong, X. -G. Wen, and M. Soljačić, Phys. Rev. B **77**, 235125 (2008).
  - <sup>2</sup> K. Sun and E. Fradkin, Phys. Rev. B **78**, 245122 (2008).
  - <sup>3</sup> K. Sun, H. Yao, E. Fradkin, and S. A. Kivelson, Phys. Rev. Lett. **103**, 046811 (2009).
  - <sup>4</sup> V. Cvetković, R. E. Throckmorton, and O. Vafek, Phys. Rev. B **86**, 075467 (2012).
  - <sup>5</sup> J. M. Murray and O. Vafek, Phys. Rev. B **89**, 201110(R) (2014).
  - <sup>6</sup> J. M. Murray, O. Vafek, and L. Balents, Phys. Rev. B **92**, 035137 (2015).
  - <sup>7</sup> I. F. Herbut, Phys. Rev. B **85**, 085304 (2012).
  - <sup>8</sup> I. F. Herbut and L. Janssen, Phys. Rev. Lett. **113**, 106401 (2014).
  - <sup>9</sup> L. Janssen and I. F. Herbut, Phys. Rev. B **89**, 205403 (2014).
  - <sup>10</sup> L. Janssen and I. F. Herbut, Phys. Rev. B **92**, 045117 (2015).
  - <sup>11</sup> I. Boettcher and I. F. Herbut, Phys. Rev. B **93**, 205138 (2016).
  - <sup>12</sup> L. Janssen and I. F. Herbut, Phys. Rev. B **95**, 075101 (2017).
  - <sup>13</sup> I. Boettcher and I. F. Herbut, Phys. Rev. B **95**, 075149 (2017).
  - <sup>14</sup> R. M. Nandkishore and S. A. Parameswaran, Phys. Rev. B **95**, 205106 (2017).
  - <sup>15</sup> I. Mandal and R. M. Nandkishore, Phys. Rev. B **97**, 125121 (2018).
  - <sup>16</sup> Y.-P. Lin and R. M. Nandkishore, Phys. Rev. B **97**, 134521 (2018).
  - <sup>17</sup> I. Mandal, Annals of Physics **392**, 179 (2018).
  - <sup>18</sup> A. Altland and B. Simons, *Condensed Matter Field Theory* (Cambridge University Press, Cambridge, 2006).
  - <sup>19</sup> A. H. Castro Neto, F. Guinea, N. M. R. Peres, K. S. Novoselov, and A. K. Geim, Rev. Mod. Phys. **81**, 109 (2009).
  - <sup>20</sup> J. Nilsson, A. H. Castro Neto, F. Guinea, and N. M. R. Peres, Phys. Rev. B **78**, 045405 (2008).
  - <sup>21</sup> R. Nandkishore and L. Levitov, Phys. Rev. B **82**, 115124 (2010).
  - <sup>22</sup> F. Zhang, J. Jung, G. A. Fiete, Q. Niu, and A. H. MacDonald, Phys. Rev. Lett. **106**, 156801 (2011).
  - <sup>23</sup> Y. Lemonik, I. Aleiner, and V. I. Fal'ko, Phys. Rev. B **85**, 245451 (2012).
  - <sup>24</sup> F. Zhang, H. Min, and A. H. MacDonald, Phys. Rev. B **86**, 155128 (2012).
  - <sup>25</sup> J. Sinova, D. Culcer, Q. Niu, N. A. Sinitsyn, T. Jungwirth, and A. H. MacDonald, Phys. Rev. Lett. **92**, 126603 (2004).
  - <sup>26</sup> S. Murakami, N. Nagaosa, and S. C. Zhang, Science **301**, 1348 (2003).
  - <sup>27</sup> J. Hirsch, Phys. Rev. Lett. **83**, 1834 (1999).
  - <sup>28</sup> C. L. Kane and E. J. Mele, Phys. Rev. Lett. **95**, 146802 (2005).
  - <sup>29</sup> B. A. Bernevig, J. Orenstein, and S.-C. Zhang, Phys. Rev. Lett. **97**, 236601 (2006).
  - <sup>30</sup> B. A. Bernevig, T. L. Hughes, and S.-C. Zhang, Science **314**, 1757 (2006).
  - <sup>31</sup> J. Wang, C. Ortix, J. van den Brink, and D. V. Efremov, Phys. Rev. B **96**, 201104(R) (2017).
  - <sup>32</sup> I. Mandal and S. Gemsheim, arXiv: cond-mat.str-el/1808.03560 (2018).
  - <sup>33</sup> J. M. Luttinger, Phys. Rev. **102**, 1030 (1956).
  - <sup>34</sup> S. Murakami, N. Nagosa, and S.-C. Zhang, Phys. Rev. B **69**, 235206 (2004).
  - <sup>35</sup> I. M. Tsidilkovski, *Electron Spectrum of Gapless Semiconductors* (Springer-Verlag, Berlin, 1997).
  - <sup>36</sup> E. -G. Moon, C. Xu, Y. B. Kim, and L. Balents, Phys. Rev. Lett. **111**, 206401 (2013).
  - <sup>37</sup> W. Witczak-Krempa, G. Chen, Y. B. Kim, and L. Balents, Annu. Rev. Condens. Matter Phys. **5**, 57 (2014).
  - <sup>38</sup> T. Kondo, M. Nakayama, R. Chen, J. J. Ishikawa, E.-G. Moon, T. Yamamoto, Y. Ota, W. Malaeb, H. Kanai, Y. Nakashima, Y. Ishida, R. Yoshida, H. Yamamoto, M. Mat-

- sunami, S. Kimura, N. Inami, K. Ono, H. Kumigashira, S. Nakatsuji, L. Balents, and S. Shin, Nat. Commun. **6**, 10042 (2015).
- <sup>39</sup> L. Savary, E. -G. Moon and L. Balents, Phys. Rev. X **4**, 041027 (2014).
- <sup>40</sup> L. Savary, J. Ruhman, J. W. F. Venderbos, L. Fu, and P. A. Lee, Phys. Rev. B **96**, 214514 (2017).
- <sup>41</sup> H. Oh, S. Lee, Y. -B. Kim, and E. -G. Moon, arXiv: cond-mat.str-el/1811.00021 (2018).
- <sup>42</sup> H. -H. Lai, B. Roy, and P. Goswami, arXiv: 1409.8675 (2014).
- <sup>43</sup> P. Goswami, B. Roy, and S. Das Sarma, Phys. Rev. B **95**, 085120 (2017).
- <sup>44</sup> A. L. Szabo, R. Moessner, and B. Roy, arXiv:1811.12415 (2018).
- <sup>45</sup> B. Roy, S. A. Akbar Ghorashi, M. S. Foster, and A. H. Nevidomskyy, Phys. Rev. B **99** 054505 (2019).
- <sup>46</sup> I. F. Herbut, Phys. Rev. Lett. **97**, 146401 (2006).
- <sup>47</sup> K. G. Wilson, Rev. Mod. Phys. **47** 773 (1975).
- <sup>48</sup> J. Polchinski, arXiv: hep-th/9210046 (1992).
- <sup>49</sup> R. Shankar, Rev. Mod. Phys. **66**, 129 (1994).
- <sup>50</sup> I. Herbut, *A Modern Approach to Critical Phenomena* (Cambridge University Press, Cambridge, England, 2007).
- <sup>51</sup> Y. Huh and S. Sachdev, Phys. Rev. B **78**, 064512 (2008).
- <sup>52</sup> J. -H. She, J. Zaanen, A. R. Bishop, and A. V. Balatsky, Phys. Rev. B **82**, 165128 (2010).
- <sup>53</sup> J. -H. She, M. J. Lawler, and E.-A. Kim, Phys. Rev. B **92**, 035112 (2015).
- <sup>54</sup> J. Wang and G.-Z. Liu, New J. Phys. **13**, 073039 (2013).
- <sup>55</sup> J. Wang and G.-Z. Liu, Phys. Rev. D **90**, 125015 (2014).
- <sup>56</sup> J. Wang and G.-Z. Liu, Phys. Rev. B **92**, 184510 (2015).
- <sup>57</sup> J. Wang, G.-Z. Liu, D. V. Efremov, and J. van den Brink, Phys. Rev. B **95**, 024511 (2017).
- <sup>58</sup> J. Wang, G. -Z. Liu, and H. Kleinert, Phys. Rev. B **83**, 214503 (2011).
- <sup>59</sup> J. Wang, Phys. Rev. B **87**, 054511 (2013).
- <sup>60</sup> J. Wang, Phys. Lett. A **379** 1917 (2015).
- <sup>61</sup> J. Wang, J. Phys. Condens. Matter **30**, 125401 (2018).
- <sup>62</sup> Y. -M. Dong, D. -X. Zheng, and J. Wang, arXiv:1806.03410 (2018).
- <sup>63</sup> S. Sachdev, *Quantum Phase Transitions* (Cambridge University Press, Cambridge, UK, 1999).
- <sup>64</sup> R. M. Fernandes, A. V. Chubukov, J. Knolle, I. Eremin and J. Schmalian, Phys. Rev. B **85**, 024534 (2012).
- <sup>65</sup> R. M. Fernandes, S. Maiti, P. Wölfe, and A. V. Chubukov, Phys. Rev. Lett. **111**, 057001 (2013).
- <sup>66</sup> I. F. Herbut and Z. Tešanović, Phys. Rev. Lett. **76**, 4588 (1996).
- <sup>67</sup> I. F. Herbut and Z. Tešanović, Phys. Rev. Lett. **78**, 980 (1997).
- <sup>68</sup> L. Fu and C. L. Kane, Phys. Rev. B **76**, 045302 (2007).
- <sup>69</sup> S. Maiti and A. V. Chubukov, Phys. Rev. B **82** 214515 (2010).
- <sup>70</sup> A. V. Chubukov, M. Khodas, and R. M. Fernandes, Phys. Rev. X **6**, 041045 (2016).
- <sup>71</sup> M. Khodas and A. V. Chubukov, Phys. Rev. B **94** 115159 (2016).
- <sup>72</sup> R. Ganesh, G. Baskaran, J. van den Brink, and D. V. Efremov, Phys. Rev. Lett. **113**, 177001 (2014).